Süleyman Demirel Üniversitesi
Fen Bilimleri Enstitüsü Dergisi
Cilt 22, Sayı 2, 397-401, 2018

Süleyman Demirel University
Journal of Natural and Applied Sciences
Volume 22, Issue 2, 397-401, 2018

DOI: 10.19113/sdufbed.58150

Hydrothermal Synthesis of Cuprous Oxide Nanoflowers and Characterization of Their Optical Properties

Aziz GENÇ*[1]

[1]Bartın University, Faculty of Engineering, Department of Metallurgical and Materials Engineering, 74100, Bartın

(Alınış / Received: 23.08.2017, Kabul / Accepted: 12.03.2018, Online Yayınlanma / Published Online: 05.04.2018)

Keywords
Cuprous oxide,
Hydrothermal synthesis,
Microstructure,
Optical properties

Abstract: In this study, the facile, one-step synthesis of cuprous oxide nanostructures via hydrothermal reaction is reported. Nanoflower-like cuprous oxides with average sizes of ~230 nm are synthesized by using copper (Cu) acetate monohydrate as the Cu source, glucose as the reducing agent and polyvinylpyrrolidone (PVP) as the surfactant in basic aqueous solutions at 140°C for 6 h. The effects of the NaOH content on the morphology of synthesized structures are also investigated, where hexapods were synthesized when no NaOH used and submicron sized octahedra were obtained with increased NaOH amount. The optical properties of the synthesized structures are studied by using photoluminescence (PL) and UV-Vis spectroscopy. PL spectra revealed the presence of different band edge emissions located at similar wavelengths for all the three samples, where the intensity of the emissions varied from sample to sample. An absorbance peak located at ~355 nm and a direct bandgap value of about Eg = 2.16 eV are measured via UV-Vis spectroscopy of the nanoflower-like cuprous oxides.

Bakır Oksit Nanoçiçeklerin Hidrotermal Sentezi ve Optik Özelliklerinin Karakterizasyonu

Anahtar Kelimeler
Bakır oksit,
Hidrotermal sentez,
Mikroyapı,
Optik özellikler

Özet: Bu çalışmada, bakır oksit nanoyapıların basit ve tek seferde hidrotermal yöntem ile sentezi rapor edildi. Ortalama ~230 nm boyutlara sahip nanoçiçek benzeri bakır oksit yapıları bakır (Cu) asetatın bakır kaynağı, glükozun redükleyici ajan ve polivinilpirolidonun (PVP) yüzey aktif madde olarak kullanıldığı bazik sulu çözelti içerisinde 140°C'de 6 saat sürede sentezlendi. Ek olarak, NaOH içeriğinin sentezlenen yapıların morfolojileri üzerindeki etkileri incelendi ve hiç NaOH kullanılmadığı zaman altıayaklı yapıların oluştuğu, NaOH oranı arttırıldığında ise mikron altı boyutlara sahip sekizyüzlülerin oluştuğu gözlemlendi. Sentezlenen yapıların optik özellikleri fotolüminisans (PL) ve UV-Vis spektroskopileri kullanarak incelendi. PL spektroskopisi her üç numune için de benzer dalga boylarına sahip, şiddetleri numuneden numuneye değişen, farklı bant kenar ışımalarının varlığını ortaya koydu. Nanoçiçek benzeri bakır oksit yapıları için yaklaşık 355 nm'de yer alan bir absorbans piki ve yaklaşık Eg = 2.16 eV olan bir doğrudan bant aralığı değeri UV-Vis spektroskopisi kullanılarak ölçüldü.

1. Introduction

Among various semiconductor oxides used in technological applications, cuprous oxide (Cu_2O) is received considerable attraction as a p-type semiconductor with a direct bandgap of 2.17 eV [1, 2]. Such a direct bandgap in the visible region, along with its high optical absorption coefficient and interesting excitonic features, make cuprous oxide an ideal candidate for solar energy conversion applications such as photovoltaics and photocatalysis [3-8]. Moreover, thanks to its low production cost and nontoxicity, cuprous oxides have been used in different applications such as gas sensors, antibacterial materials, electrodes for Li-ion batteries etc. [9-12].

The performances of cuprous oxide nanostructures in different applications are found to be highly dependent on their morphology [2, 3, 7, 11]. For this

* Corresponding author: agenc@bartin.edu.tr

reason, extensive studies have been conducted in order to fabricate cuprous oxides with various shapes such as nanospheres [10], nanocubes [13], nanowires [14], octahedra [15], multipods [16], nanoflowers [17] etc. Different techniques including wet chemical reduction, hydrothermal synthesis and electrodeposition have been utilized to synthesize shape selective cuprous oxide nanostructures [1, 10, 14, 16]. In this study, hydrothermal synthesis route is used for its simplicity and ability to finely control the morphology of the products by tuning the parameters of the synthesis [18]. One-pot synthesis of cuprous oxide nanostructures with nanoflower-like and octahedral morphologies via hydrothermal reactions at 140°C for 6 h is reported.

2. Material and Method

Syntheses of cuprous oxide nanostructures were realized by using a single step hydrothermal method. As Cu source, 600 mg Copper Acetate Monohydrate ($C_4H_6CuO_4.H_2O$, Sigma Aldrich, CAS No: 6046-93-1) was dissolved in 15 ml distilled water at room temperature by vigorous stirring (800 rpm). Separately, 108 mg D(+)-Glucose ($C_6H_{12}O_6$, Merck, CAS No: 50-99-7) and 1 g Polyvinylpyrrolidone (PVP, $(C_6H_9NO)_n$, average mol wt 40000, Sigma Aldrich, CAS No: 9003-39-8) were dissolved in 30 ml distilled water and these two solutions were mixed. 200 mg sodium hydroxide (NaOH, Merck, CAS No:1310-73-2) was dissolved in 5 ml distilled water and was added dropwise to the main solution. Obtained 50 ml solution was transferred to 100 ml teflon lined stainless-steel autoclave giving a filling rate of 50%. The hydrothermal synthesis is conducted in a furnace at 140°C for 6 h under autogeneous pressures. After the hydrothermal synthesis, products were purified by centrifuging (Electro-mag M4812P) at 5000 rpm with distilled water/ethanol solutions for three times and the powders were obtained by drying overnight at 65°C. The sample synthesized by using the above procedure was named as the Sample #1. Two other samples were synthesized using similar procedures except the NaOH amount. Sample #2 was synthesized without using any NaOH and the sample #3 was synthesized by using 400 mg NaOH under the same experimental conditions.

Phase characterizations of the obtained products were conducted using a RIGAKU SmartLab™ X-ray diffractometer (XRD) with Cu Kα radiation. Microstructural characterizations were conducted using a TESCAN™ MAIA XMU scanning electron microscope (SEM). The samples are coated with a few nm thick Au-Pd prior to SEM examination in order to prevent charge accumulations on the surface of the samples. An accelaration voltage of 5 kV is used for SEM measurements and an accelaration voltage of 30 kV scanning transmission electron microscopy (STEM) measurement. Average size for the sample #1 is calculated via measuring at least 200 nanoparticles from different SEM images by using ImageJ freeware and the results are presented with standard deviations.

Optical properties of the samples were characterized by using photoluminescence (PL) and UV-Vis spectroscopy measurements. For both PL and UV-Vis measurements, a few mg of the samples was dispersed in absolute ethanol via ultrasonication and their optical properties are measured against a reference of absolute ethanol. The concentrations of the solutions were adjusted with absolute ethanol in order to have similar emission/absorbance counts before the experiments. PL is conducted by using an EDINBURGH INSTRUMENTS™ FS5 fluorescence spectrometer with an excitation wavelength of 300 nm. The PL spectra are recorded between 400 nm and 650 nm with a resolution of 0.5 nm. UV-Vis spectroscopy measurements are conducted by using a Shimadzu UV-3600 UV-Vis-NIR spectrophotometer equipment. The UV-Vis spectra of the samples are recorded between 250 nm and 750 nm, with a resolution of 2 nm (the reason for using such a low resolution was the precipitation tendency of micron sized cuprous oxides in absolute ethanol solutions).

3. Results and Discussions

Figure 1 shows the microstructures of the synthesized cuprous oxide nanoflowers. Fig. 1a, 1b and 1c are SEM images obtained from the sample #1 at different magnifications, revealing that the sample consists nanoflower like structures with average sizes of 230 ± 42 nm (obtained by measuring at least 200 nanoparticles from various SEM images). Higher magnification (300kx) SEM image shown in Fig. 1c reveal that these flower like nanostructures are composed of small nanocrystallites with ~20 nm sizes. Fig. 1d is a bright field (BF) scanning transmission electron microscope (STEM) image of sample #1, obtained in order to reveal the porous surface structure of the nanoflowers.

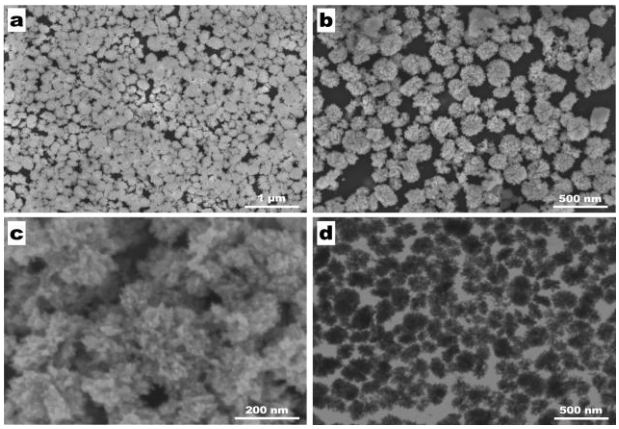

Figure 1. a), b) and c) SEM images obtained from the sample #1 at different magnifications, revealing the presence of the nanoflower like morphology with ~230 nm sizes. d) is a bright field STEM micrograph of the same sample, showing the porous structure.

Two other samples are fabricated using similar procedures to that of the sample #1 yet with different NaOH amounts and their morphologies are shown in Fig. 2. Fig. 2a and 2b are SEM images obtained from the sample #2, which is synthesized without any NaOH. The presence of micron sized hexapods with different growth stages, i.e. long and short leg sizes, can be clearly seen in these images. It should be noted here that micron sized hexapods are typical products obtained during hydrothermal process of Cu salts [16, 19], suggesting that the PVP used as surfactant has almost no effect for this synthesis. By comparing the microstructures obtained from sample #1 and sample #2, the presence of NaOH, thus the pH of the synthesis, is a crucial parameter during the copper oxide synthesis. In order to further investigate the effects of NaOH amount, another sample containing two times more NaOH than the sample #1 (400 mg) is synthesized and referred as sample #3. SEM images of sample #3 are given in Fig. 2c and 2d, where perfectly shaped octahedra with sizes about 1 micron can be seen. As it is obviously seen in the low magnification SEM image in Fig. 2c, octahedral particles of sample #3 are quite homogeneous both in size and shape. Increasing the amount of NaOH has drastically changed the morphology of the synthesized sample, leading the growth of octahedral particles, which can be regarded as the initial stage for the synthesis of hexapods observed for the sample #2 [16, 19].

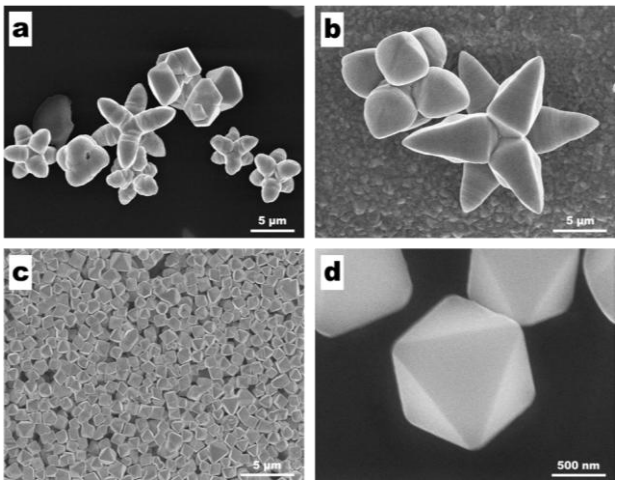

Figure 2. a) and b) are SEM images of sample #2 revealing the presence of micron sized hexapods. c) and d) are SEM images of sample #3, where octahedral particles with 1 micron sizes can be seen.

XRD patterns of the as-synthesized powders are shown in Fig. 3. As seen in the XRD pattern in Fig. 3a, main phase of the sample #1 is a cubic cuprous oxide (cuprite, Cu_2O) phase (space group: Pn-3m) with lattice parameter of a = 0.425 nm. In addition to the Cu_2O phase, the XRD pattern suggests the presence of a monocilinic CuO phase (space group: C2/c) with lattice parameters a = 0.465 nm, b = 0.341 nm and c = 0.510 nm with several low intensity peaks. Moreover, a peak corresponding to the reflections from the {111} family of planes of a metallic Cu phase (space group: Fm-3m) with lattice parameter of a = 0.360 nm is observed in this XRD pattern. The XRD pattern obtained from the sample #2 is shown in Fig. 3b, revealing the presence of diffraction peaks of only the Cu_2O phase. The sample #3 is also mainly composed of the Cu_2O phase, whereas the presence of a peak belonging to the metallic Cu phase is also visible in the XRD pattern (Fig. 3c). These XRD patterns reveal that the synthesized nanostructures are mainly cuprous oxide with occasional presence of CuO and metallic Cu. Presence of these two phases may indicate the different reduction/oxidation reactions taking place during the hydrothermal process, where the main phase is the sub-stoichiometric cuprous oxide phase.

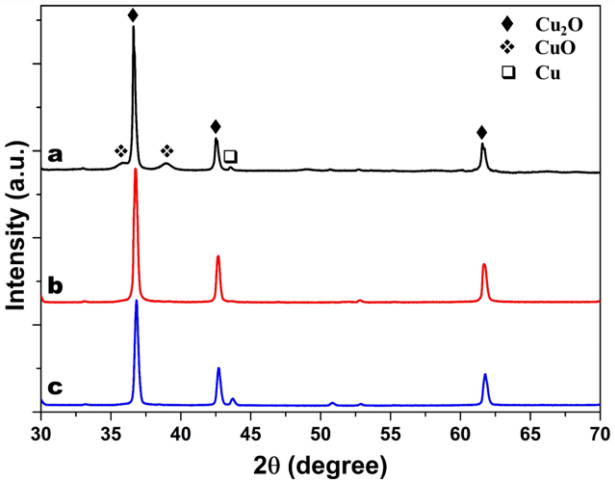

Figure 3. XRD patterns of the synthesized samples. a) Sample #1, b) sample #2 and c) sample #3

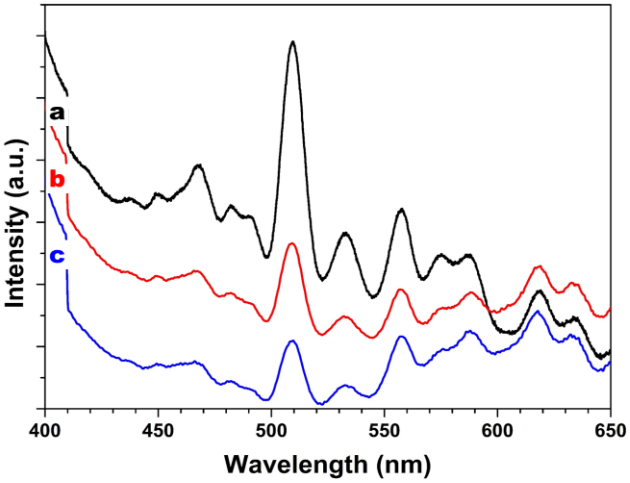

Figure 4. Room temperature PL spectra of the synthesized samples. a) Sample #1 (in black), b) sample #2 (in red) and c) sample #3 (in blue).

Figure 4a shows the room temperature PL spectrum between 400 nm and 650 nm obtained from the sample #1 with an excitation wavelength of 300 nm. As seen in this spectrum (in black), many different peaks, some of which are very-well defined, corresponding to blue, green, yellow and orange emissions are observed. The observed emission

peaks are located around 438 nm (2.83 eV), 450 nm (2.75 eV), 468 nm (2.65 eV), 482 nm (2.57 eV), 510 nm (2.43 eV), 533 nm (2.33 eV), 558 nm (2.22 eV), 576 nm (2.15 eV), 589 nm (2.10 eV), 619 nm (2.00 eV) and 633 nm (1.96 eV). These band edge emissions, considered as a series of Wanier hydrogen-like excitonic transitions, are attributed to the excitonic transitions from different sub-levels of the conduction band to the Cu d-shells of the valence band and some defects-related emissions [20, 21, 22]. Surprisingly, PL spectra obtained from the other two samples (Fig. 4b for the sample #2 (in red) and Fig. 4c for the sample #3 (in blue)) also reveal the presence these emissions at the same wavelengths, suggesting that the samples have similar band edge emissions and/or defect emissions regardless of their morphologies. Yet, the emission intensities vary from sample to sample and the sample #1 with its nanostructured flower like morphology exhibits the most intense emissions.

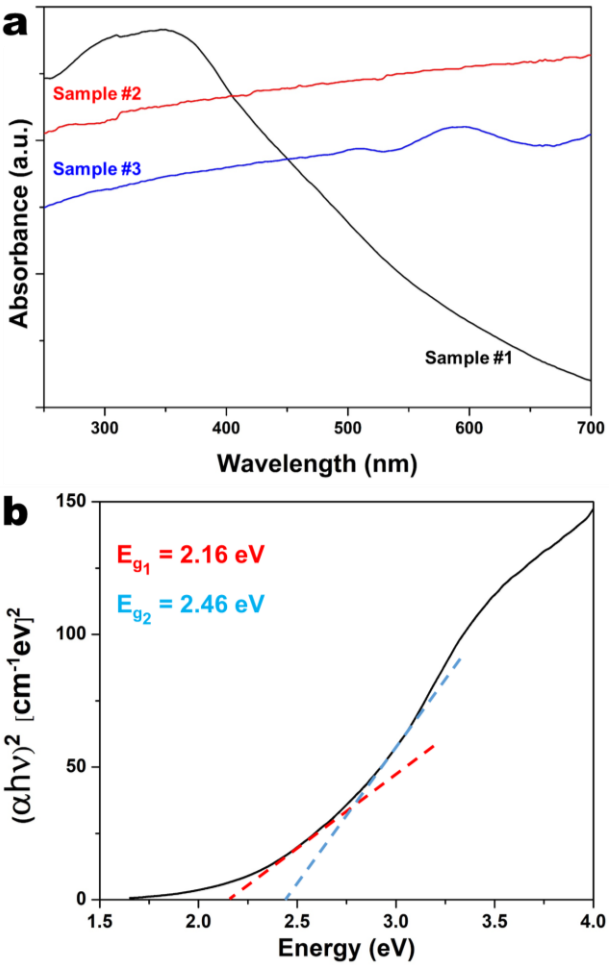

Figure 5. a) UV-Vis spectra obtained from the sample #1 (in black), sample #2 (in red) and sample #3 (in blue). b) The Tauc plot obtained from the UV-Vis spectrum of the sample #1 and two direct bandgap values determined via linear extrapolation.

Figure 5a shows the UV-Vis spectra obtained from the samples. UV-Vis spectrum obtained from the sample #1 reveals the presence of an absorbance peak located at ~355 nm, whereas the UV-Vis spectrum of the sample #2 is highly absorbing at all wavelengths without any specific features in the spectrum. This maybe due to the fact that the sample #2 consists microstructures with different shapes. The UV-Vis spectrum obtained from the sample #3 also suggests that this sample is highly absorbing at various wavelengths, yet the presence of two small absorbance peaks located at ~508 nm and ~594 nm can be observed in this spectrum. Fig. 5b shows the so-called Tauc plot [23] obtained from the UV-Vis spectrum of the sample #1. Linear extrapolation of this plot suggests that the bandgap values of the sample vary between 2.16 eV and 2.46 eV, rather than a sharp curve suggesting a very defined bandgap. This may be due to the presence of various copper oxide phases with different oxidation values (see XRD pattern in Fig. 3a), eventhough the amount of phases other than the Cu_2O seems to be scarce. Main phase for the sample #1 is reported to be the cuprous oxide (Cu_2O) and the direct bandgap value of Eg = 2.16 eV determined via linear extrapolation of the Tauc plot presented in Fig. 5b is very consistent with the reported bandgap of this phase [2].

4. Conclusions

In the present study, we report the facile synthesis of cuprous oxide nanostructures via hydrothermal synthesis at 140°C for 6 h. We have investigated the effects of NaOH content on the morphology of the synthesized products. Based on the obtained results in this study, we draw the following conditions.

1. Cuprous oxide nanostructures with flowerlike morphologies having sizes about 230 ± 42 nm could be synthesized. These structures are formed by small crystallites of ~20 nm.

2. By changing the NaOH amount, hexapods with sizes about several microns and perfectly shaped octahedra with sub-micron sizes could be obtained.

3. PL spectroscopy revealed the presence of multiple band edge emissions which are located at the same wavelengths for all three samples.

4. UV-Vis spectrum obtained from the nanoflower-like cuprous oxides revealed the presence of an absorbance peak located at ~ 355 nm, whereas two small absorbance peaks located at ~508 nm and ~594 nm were observed for the octahedral cuprous oxides. Bandgap of the flower-like nanostructures is found to vary between ~2.16 eV and ~2.46 eV.

Acknowledgment

The author wish to acknowledge the funding from Bartın University Scientific Research Projects Unit for the project entitled with "Synthesis of Hollow Metal Oxide Nanostructures and Characterizaton of Their Microstructural and Photocatalytic Properties".

References

[1] Kuo, C.H., Huang, M.H. 2010. Morphologically controlled synthesis of Cu_2O nanocrystals and their properties. Nano Today, 5 (2010), 106-116.

[2] Sun, S., Yang, Z. 2014. Recent advances in tuning crystal facets of polyhedral cuprous oxide architectures. RSC Advances, 4 (2014), 3804-3822.

[3] Zhang, L. Wang, H. 2011. Cuprous oxide Nanoshells with Geometrically Tunable Optical Properties. ACS Nano, 5 (2011), 3257-3267.

[4] Karapetyan, A., Reymers, A., Giorgio, S., Fauquet, C., Sajti, L., Nitsche, S., Nersesyan, M., Gevorgyan, V., Marine, W. 2015. Cuprous oxide thin films prepared by thermal oxidation of copper layer. Morphological and optical properties. Journal of Luminescence, 159 (2015), 325-332.

[5] Wei, H.M., Gong, H.B., Chen, L., Zi, M., Cao, B.Q. 2012. Photovoltaic Efficiency Enhancement of Cu_2O Solar Cells Achieved by Controlling Homojunction Orientation and Surface Microstructure, Journal of Physical Chemistry, 116 (2012), 10510-10515.

[6] Li, S., Ge, X., Jiang, S., Peng, X., Zhang, Z., Li, W., Yu, S. 2015. Synthesis of octahedral and cubic Cu_2O microcrystals in sub- and super-critical methanol and their photocatalytic performance. Journal of Materials Science, 50 (2015), 4115-4121.

[7] Li, R., Yan, X., Yu, L., Zhang, Z., Tang, Q., Pan, Y. 2013. The morphology dependence of cuprous oxide and its photocatalytic properties. CrystEngComm, 15 (2013), 10049-10058.

[8] Han, K., Tao, M. 2009. Electrochemically deposited p-n homojunction cuprous oxide solar cells. Solar Energy Materials & Solar Cells, 93 (2009), 153-157.

[9] Zhang, H., Zhu, Q,. Zhang, Y., Wang, Y., Zhao, L., Yu, B. 2007. One-Pot Synthesis and Hierarchical Assembly of Hollow Cu_2O Microspheres with Nanocrystals-Composed Multishell and Their Gas-Sensing Properties. Advanced Functional Materials, 17 (2007), 2766-2771.

[10] Zhang, J., Liu, J., Peng, Q., Wang, X., Li, Y. 2006. Nearly Monodisperse Cu_2O and CuO Nanospheres: Preparation and Applications for Sensitive Gas Sensors. Chemistry of Materials, 18 (2006), 867-871.

[11] Pang, H., Gao, F., Lu, Q. 2009. Morphology effect on antibacterial activity of cuprous oxide. Chemical Communications, (2009), 1076-1078.

[12] Poizot, P., Laruelle, S., Grugeon, S., Dupont, L., Tarascon, J.M. 2000. Nano-sized transition-metal oxides as negative-electrode materials for lithium-ion batteries. Nature, 407 (2000), 496-499.

[13] Gou, L., Murphy, C.J. 2004. Controlling the size of Cu_2O nanocubes from 200 to 25 nm. Journal of Materials Chemistry, 14 (2004), 735-738.

[14] Ko, E., Choi, J., Okamoto, K., Tak, Y., Lee, J. 2006. Cu_2O Nanowires in an Alumina Template: Electrochemical Conditions for the Synthesis and Photoluminescence Characteristics. Chemical Physics Physical Chemistry, 7 (2006), 1505-1509.

[15] Nguyen, M.A., Bedford, N.M., Ren, Y., Zahran, E.M., Goodin, R.C., Chagani, F.F., Bachas, L.G., Knecht, M.R. 2015. Direct Synthetic Control over the Size, Composition, and Photocatalytic Activity of Octahedral Copper Oxide Materials: Correlation Between Surface Structure and Catalytic Functionality. ACS Applied Materials Interfaces, 7 (2015), 13238-13250.

[16] Ghosh, S., Das, R., Naskar, M.K. 2016. Morphological evolution of hexapod Cu_2O microcrystals by a rapid template-free autoclaving technique. Materials Letters, 183 (2016), 325-328.

[17] Zhang, L., Yuan, F., Zhang, X., Yang, L. 2011. Facile synthesis of flower like copper oxide and their application to hydrogen peroxide and nitrite sensing. Chemistry Central Journal, 5 (2011), 75.

[18] Einarsrud, M.A., Grande, T. 2014. 1D oxide nanostructures from chemical solutions. Chemical Society Reviews, 43 (2014), 2187-2199.

[19] Zhang, X., Xie, Y., Xu, F., Xu, D., Liu, H. 2004. Growth and morphological evolution of hexapod-shaped cuprous oxide microcrystals at room temperature, Canadian Journal of Chemistry, 82 (2004), 1341-1345.

[20] Das, K., De, S.K. 2009. Optical and photoconductivity studies of Cu_2O nanowires synthesized by solvothermal method. Journal of Luminescence, 129 (2009), 1015-1022.

[21] Wei, H., Gong, H., Wang, Y., Hu, X., Chen, L., Xu, H., Liu, P., Cao, B. 2011. Three kinds of Cu_2O/ZnO heterostructure solar cells fabricated with electrochemical deposition and their structure-related photovoltaic properties. Cryst. Eng. Comm., 13 (2011), 6065-6070.

[22] No, Y.S., Oh, D.H., Kim, S.Y., Yoo, K.H., Kim, T.W. 2012. Structural, optical, and electrical properties of Cu_2O nanocubes grown on indium-tin-oxide-coated glass substrates by using seed-layer-free electrochemical deposition method. Applied Surface Science, 258 (2012), 7581-7583.

[23] Tauc, J., Grigorovici, R., Vancu, A. 1966. Optical Properties and Electronic Structure of Amorphous Germanium. Physica Status Solidi, 15 (1966), 628-637.